NANO EXPRESS

PAPER

A novel approach to the green synthesis of zinc oxide nanorods using Thymus kotschyanus plant extract: effect of ammonium hydroxide and precursor concentration

Peyman K Aspoukeh[1], **Azeez A Barzinjy**[1,2,*] **and Samir M Hamad**[1]

[1] Scientific Research Centre, Soran University, Kurdistan Region, Iraq
[2] Physics Education Department, Faculty of Education, Tishk International University, Erbil, Iraq
* Author to whom any correspondence should be addressed.

E-mail: azeez.azeez@soran.edu.iq

Keywords: zinc oxide nanorods, green synthesis method, Thymus kotschyanus plant extract, ammonium hydroxide, nanorods alignment

OPEN ACCESS

RECEIVED
22 August 2023

REVISED
22 September 2023

ACCEPTED FOR PUBLICATION
28 September 2023

PUBLISHED
13 October 2023

Abstract

This research introduces a pioneering green method for synthesizing zinc oxide nanorods (ZnO NRs) on a glass substrate using Thymus kotschyanus plant extract. The study delves into the intricate effects of ammonium hydroxide and precursor concentrations on the morphology, size, alignment, and crystalline structure of ZnO NRs. Through systematic experimentation, it was found that specific concentrations of these substances play vital roles in the formation and properties of the nanorods. Notably, a low concentration of the precursor coupled with a high concentration of ammonium hydroxide led to well-aligned hexagonal ZnO NRs with a remarkable aspect ratio. Variations in these concentrations were also found to influence the length, diameter, and alignment of the nanorods. The findings were corroborated using a diverse array of analytical techniques, including transmission and scanning electron microscopy, x-ray diffraction, UV–vis spectroscopy, and energy-dispersive x-ray analysis. The UV–vis spectra provided further insights into the optical properties and band gap energy of the ZnO NPs, while EDX analysis confirmed the elemental composition. This work represents a significant advancement in eco-friendly nanomaterial synthesis, providing detailed insights into the controlled fabrication of aligned ZnO NRs. Its innovative approach and extensive investigation into influencing factors make it a valuable contribution to the field of nanoscience.

1. Introduction

Zinc oxide (ZnO) is recognized as an n-type semiconductor, characterized by its hexagonal wurtzite crystalline formation and a direct bandgap of around 3.37 eV. Moreover, it exhibits a substantial exciton binding energy, measuring 60 meV at ambient temperature [1–3]. These distinctive attributes render ZnO suitable for a wide array of technological applications, encompassing gas detection sensors [4], photodetection devices [5], dye-based solar cells [6], transparent electrical conductors [7], devices that exploit piezoelectric effects [8], high-capacity electronic systems [9], thin-film transistor technology [10], light-emitting applications [11], and various solar cell configurations [12].

The synthesis of ZnO can lead to a plethora of nanostructured morphologies, ranging from nanoparticles and nanosheets to more complex structures like nanotubes, nanowires, nanoarrays, nanodisks, nanobelts, nanorods, and nanorings [13]. Among these, one-dimensional (1D) configurations of ZnO, including rods, wires, and needles, stand out for their extraordinary properties. These 1D structures hold significant potential for integration into various devices, with applications spanning the fields of electrical engineering, optoelectronics, electrochemistry, and electromechanical systems [14]. In particular, nanorods such as ZnO NRs, typified by their solid elongated form, represent a notable subclass of 1D nanostructures.

Zinc oxide nanorods (ZnO NRs) have garnered substantial attention in scientific research, owing to a set of distinct physical and chemical characteristics. These include a pronounced aspect ratio, an expansive surface

area, and superior optical and electrical behaviors [15]. The wurtzite structure of ZnO NRs manifests in a unique hexagonal form, where the polar face aligns with the 002 plane, and the non-polar faces correspond to the 100 and 101 planes.

The crystal rod's growth is predominantly facilitated along the *c*-axis, a feature that stems from the positioning of the polar face. This growth behavior can be explained by the comparatively weaker thermodynamic stability of surface dipoles found on the polar faces relative to the non-polar ones [16]. Throughout the crystallization process, the polar facets actively engage with zinc hydroxyl ($Zn(OH)_2$) and hydroxyl (OH) ions. These ions play a crucial role, functioning as the elementary components for the structure's formation [17].

The synthesis of zinc oxide nanorods (ZnO NRs) can be achieved through various methods, including molecular beam epitaxy [18], hydrothermal techniques [19], pulsed laser deposition [20], vapor–liquid–solid processes [21], laser-induced catalytic growth [22], and chemical bath deposition [23]. Among these, hydrothermal synthesis has gained popularity in the creation of ZnO NRs, prized for its straightforward approach, economic viability, and the control it offers over the NRs' size and shape by manipulating reaction parameters [24].

Similarly, the sol–gel process has demonstrated its efficacy in producing ZnO NRs, yielding products of high purity, uniformity, and crystalline quality [25]. Vapor deposition techniques, including chemical vapor deposition (CVD) [10] and physical vapor deposition (PVD) [26, 27], have also been employed to synthesize ZnO NRs with controlled and superior characteristics. These methods, however, are often constrained by the necessity for hazardous and costly chemicals, elevated temperatures, and intricate equipment, restricting their broader application.

In recent times, green synthesis methods have surfaced as an appealing alternative, providing several benefits such as affordability, environmental compatibility, and the absence of harmful chemicals. These eco-friendly approaches utilize biological agents like plant extracts, bacteria, and fungi as both reducing and stabilizing agents. Examples include the use of botanical extracts from tea, pomegranate, and ginger for the formation of metal or metal oxide nanoparticles. Furthermore, green synthesis techniques may incorporate natural compounds such as flavonoids, polyphenols, enzymes, and proteins to facilitate the generation of nanoparticles [28].

The synthesis of zinc oxide nanorods (ZnO NRs) through green methods is typically a two-step process involving nucleation and subsequent particle growth. The starting solution often consists of zinc nitrate hexahydrate mixed with phytochemicals derived from plant extracts, all dissolved in double-distilled water. To control the solution's pH, usually maintained between 7 and 10 where hydroxyl (OH^-) ions are prevalent, a base such as sodium hydroxide or ammonium is commonly employed as a buffering agent [29].

This research represents a pioneering exploration in the field. To the best of the authors' knowledge, it constitutes the first initiative to leverage the green method in both the preparation of seed layers and the alignment of ZnO NRs growth on a glass substrate, as opposed to conventional methodologies. The study not only characterizes the green-synthesized ZnO NRs but also delves into the influence of deposition factors such as precursor and ammonium concentration on the NRs' morphology and orientation. Furthermore, the authors envision that this extensive investigation heralds new opportunities to apply a wholly green method for fabricating nanorods from various other materials.

The growth mechanism of ZnO NRs using the green method requires two steps, nucleation and growth of the particles. A solution mixture of zinc nitrate hexahydrate and phytochemicals from plant extraction in double-distilled water is typically used for the synthesis of ZnO NRs. Most often, a base such as sodium hydroxide or ammonium is utilized to act as a pH buffer and control a solution's pH between 7 and 10, where hydroxyl (OH^-) ions are abundant [29].

2. Experimental and methods

2.1. Materials

In the course of this research, the utilization of high-purity analytical reagents and specialized laboratory apparatus was essential. The chemicals employed, including zinc acetate dihydrate ($Zn(CH_3CO_2)_2$), zinc nitrate hexahydrate ($Zn(NO_3)6H_2O$), ammonium solution (25%) and ethanol, were sourced from Merck. Additionally, the dried Thymus kotschyanus plant, a crucial component in the synthesis, was procured from Piranshahr city, located at coordinates 36.6931° N, 45.1439° E, in Iran. Throughout the experimental process, double-distilled water (DDW) and all other solvents were employed as received, without any further purification steps.

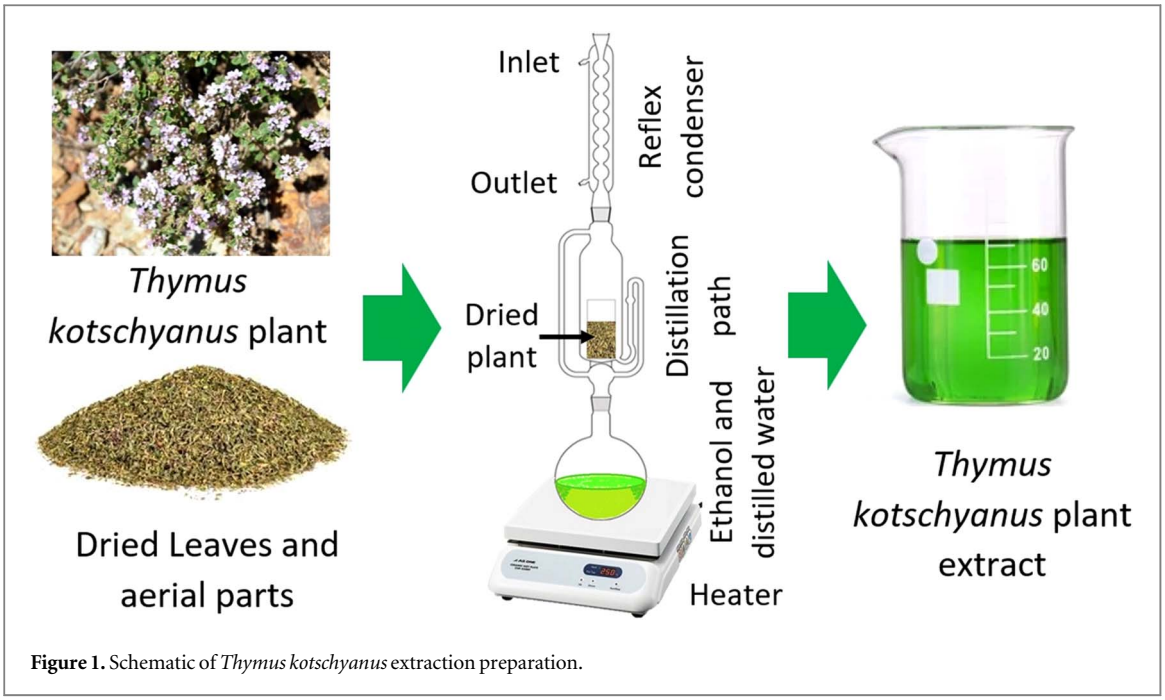

Figure 1. Schematic of *Thymus kotschyanus* extraction preparation.

2.2. Plant extract preparation

Within the scope of this investigation, the extract of the Thymus kotschyanus plant was employed as a natural means to synthesize nanoparticles (NPs). Belonging to the Labiatae family, the Thymus genus encompasses over 215 species, primarily characterized as herbaceous perennials [30]. Historically, various Thymus species have found application in medicinal contexts, specifically through the use of aerial parts and volatile constituents. These applications extend to the manufacturing of herbal beverages, flavoring agents, and spices [31].

The extract of Thymus kotschyanus is particularly rich in essential oils and phenolic compounds, such as carvacrol and thymol, which are known for their antioxidant attributes [32]. Thymol, recognized as a prominent constituent of the Thymus L. extract, has been identified as an effective capping and stabilizing agent in the formation of ZnO nanostructures [33]. Additionally, research has revealed that thymol, in conjunction with other polyphenolic compounds, plays a vital role in inhibiting agglomeration and shaping the crystal structure during the ZnO NPs synthesis process [34].

The organic materials from Thymus kotschyanus plant were extracted using the Soxhlet extraction method. The process began with a pre-extraction stage, lasting one hour, involving the use of a solvent, thimble, glass wool, and boiling chips (as illustrated in figure 1). For the main extraction, 20 grams of the dried and pulverized Thymus kotschyanus plant were enclosed in a thimble, cushioned with glass wool, and placed within the extractor chamber. A mixture of ethanol and distilled water, in a 60:40 ratio, totaling 250 ml, was poured into a round-bottom flask containing boiling chips to ensure uniform boiling throughout the extraction. This stage endured for one hour, after which the resultant mixture was reduced to half its original volume through solvent evaporation, employing a rotary evaporator [35]. The resulting dark green extract was then cooled to 25 °C, filtered through filter paper, and conserved in a refrigerator at 4 °C for future use. Such preservation conditions not only prolong the extract's analytical usability but also mitigate alterations in the biological molecules' activities within the extract, which might otherwise distort their representation of *in vivo* processes.

2.3. Seed Layer preparation using green synthesized ZnO NPs

Following the extraction phase, the experiment proceeded with the preparation of 50 ml of Thymus kotschyanus plant extract, to which zinc acetate dihydrate, $Zn(CH_3COO)_2(H_2O)_2$, was added at 0.5 M concentrations. The ensuing mixture was agitated on a hot plate at 60 °C for a duration of 30 min. Simultaneously, six glass substrates were meticulously cleaned with acetone, ethanol, and distilled water, subsequently allowed to air-dry at ambient temperature.

The experiment then proceeded to the dip-coating phase, utilizing a device calibrated to a movement speed of 6 cm min^{-1}. This sequence was repeated sixfold for every substrate, culminating in an annealing process conducted in an oven for 1 h at 450 °C (figure 2).

The chemical transformations underpinning the deposition of the ZnO seed layer are described by the ensuing reactions:

Figure 2. Schematic representation of ZnO seed layer preparation on the glass substrate.

$$Zn(CH_3COO)_2 \bullet 2H_2O \xrightarrow{\text{Dissociation}} Zn^{2+} + 2CH_3COO^- + 2H_2O \quad (1)$$

$$Zn^{2+} + 2C_2H_5OH \xrightarrow{\text{Alcoholysis}} Zn(C_2H_5O)_2 + 2H^+ \quad (2)$$

$$2CH_3COO^- + 2H^+ \longrightarrow 2CH_3COOH \quad (3)$$

$$Zn(C_2H_5O)_2 + 2H_2O \xrightarrow{\text{Hydrolysis}} Zn(OH)_2 + 2C_2H_5OH \quad (4)$$

$$nZn(OH)_2 + nZn(C_2H_5O)_2 \xrightarrow{\text{Condensation}} HO\text{–}[ZnO]_n\text{—}CH_2CH_3 + nC_2H_5OH \quad (5)$$

$$HO\text{—}[ZnO]_n\text{—}CH_2CH_3 \xrightarrow{\Delta} n(ZnO) + C_2H_5OH \quad (6)$$

2.4. ZnO NRs synthesis on glass substrate

In the present study, and as depicted in figure 3, a green method was employed for the synthesis of zinc oxide nanorods (ZnO NRs). The procedure involved blending zinc nitrate hexahydrate ($Zn(NO_3)_6H_2O$) as a precursor with a prepared plant extract-based solvent, and utilizing ammonium hydroxide to regulate the pH of the mixture. To explore the influence of ammonium hydroxide on the fabrication of aligned ZnO NRs, the following experimental sequence was undertaken. At the beginning three distinct solutions were prepared in individual beakers. The first beaker was representing a solution created by dissolving 0.05 M of zinc nitrate hexahydrate in a 2:1 mixture of prepared plant extract and double-distilled water. While, the second beaker was representing a solution analogous to the first, but augmented with 0.033 M of ammonium hydroxide. The third beaker was a mixture comprising 50 ml of plant extract, 0.05 M of zinc nitrate hexahydrate, and 0.335 M of ammonium hydroxide, adhering to the prescribed ratio of plant extract to double-distilled water. The mixed solutions were agitated on a hotplate set to 60 °C for 15 min. A seeded substrate was then immersed in each beaker containing the respective solutions. The solutions and substrates were relocated to an oven preheated to 90 °C and remained there for three hours. The substrates were left to air-dry at room temperature, followed by calcination in a furnace at 450 °C for two hours. Optimization and Concentration Variation: Upon determining the optimal synthesis method for the nanorods, three different concentrations (0.02, 0.05, and 0.1 M) of zinc nitrate hexahydrate precursor were prepared. The aim of this phase was to scrutinize the effect of precursor concentration, regarded as a secondary parameter, on the formation of well-aligned nanorods [36].

The chemical processes underlying the creation of ZnO NRs can be encapsulated in the following reactions [37]:

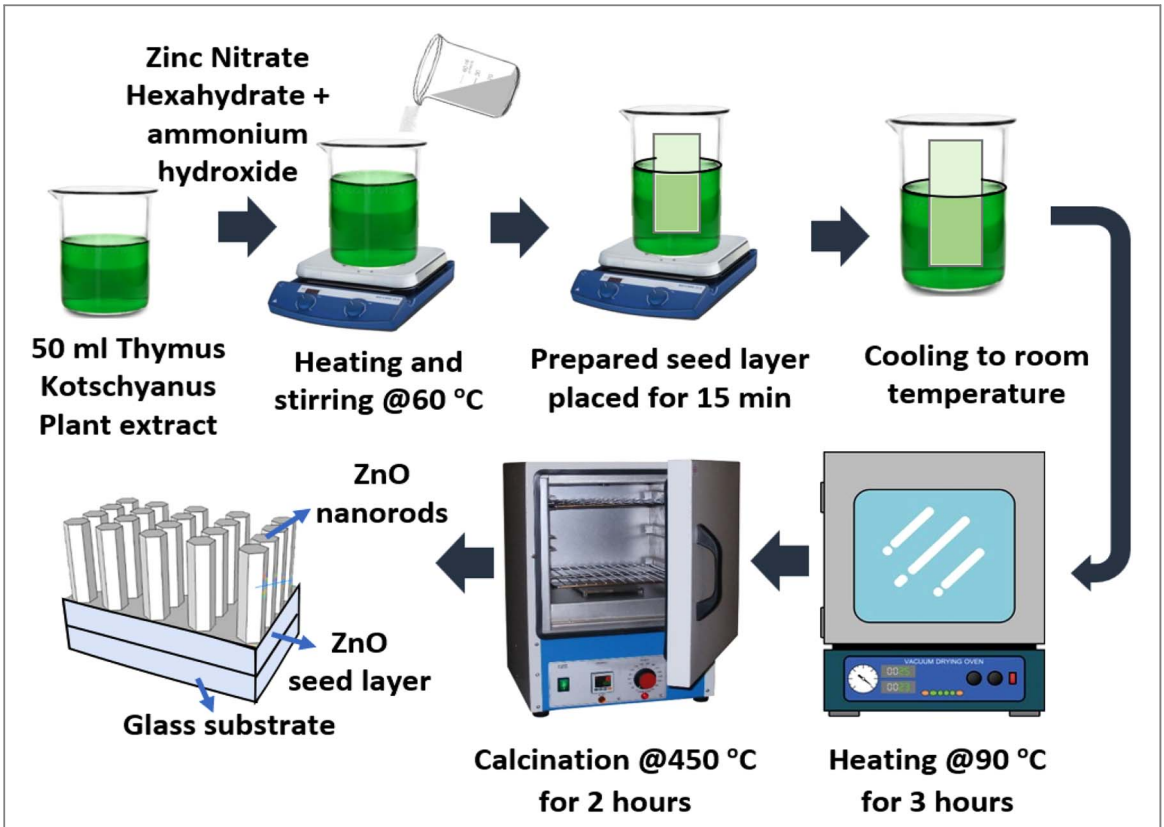

Figure 3. Schematic diagram of the green growth process of ZnO NRs on the glass substrate.

$$Zn(NO_3)_2 \bullet 6H_2O \longrightarrow Zn^{2+} + 2NO_3^- + 6H_2O \quad (7)$$

$$C_6H_{12}N_4 + 6H_2O \longrightarrow 6HCHO + 4NH_3 \quad (8)$$

$$NH_3 + H_2O \longrightarrow NH_4^+ + OH^- \quad (9)$$

$$2OH^- + Zn^{2+} \longrightarrow Zn(OH)_2 \quad (10)$$

$$Zn(OH)_2 \longrightarrow ZnO + H_2O \quad (11)$$

In the process of synthesizing zinc oxide nanorods (ZnO NRs), the incorporation of ammonium hydroxide into zinc nitrate hexahydrate ($Zn(NO_3)_2{\cdot}6H_2O$) serves dual functions: it operates both as a complexing agent and a pH regulator. These roles substantially influence the morphology and characteristics of the ensuing nanorods [38].

Formation of Complex Compound: Upon the introduction of ammonium hydroxide, it interacts with zinc nitrate hexahydrate, resulting in a complex compound. This compound subsequently dissociates, liberating Zn^{2+} ions into the solution.

The available Zn^{2+} ions react with hydroxide ions (OH^-) produced from the dissociation of ammonium hydroxide. This reaction yields $Zn(OH)_2$ species. Through a subsequent dehydration process, the $Zn(OH)_2$ species are converted into ZnO nanocrystals. These nanocrystals continue to grow along the [002] crystal direction, culminating in the nanorod structures. The deployment of ammonium hydroxide as a pH regulator is pivotal, as it elevates the solution's pH level, directly affecting the ZnO nanorods' growth rate. At higher pH values, there is an increase in hydroxide ion concentration, leading to an augmented nucleation and growth rate of the final structures.

Uniformity and Reproducibility: Additionally, the use of ammonium hydroxide contributes to maintaining a stable pH within the solution, fostering a more uniform and reproducible growth of the ZnO nanorods.

The intricate relationship between the chemical components and the controlled conditions in the synthesis process elucidates the precise manner in which the ZnO NRs are formed. The selection of agents and the understanding of their roles not only enable the desired structural formation but also offer insights into tailoring specific properties of the nanorods.

3. Characterization techniques

X-ray Diffraction (XRD) serves as a vital technique to investigate material crystallinity and structure. Experiments were conducted using a PANanalytical X'Pert PRO, scanning at 1°/min across a 2θ range of 5° to 75°, with Cu Kα radiation ($\lambda = 1.5406$ Å). UV–vis Spectrophotometry employed for qualitative and quantitative analysis, UV–vis spectrophotometry measures the absorbance of a UV–vis light beam as it traverses a sample. The synthesis of ZnO nanoparticles was verified using a Super Aquarius Spectrophotometer-2000. Scanning Electron Microscopy (SEM), utilized to examine the two-dimensional structure and surface morphology at high magnifications, SEM involves bombarding the sample with a beam of electrons. Depending on the beam's energy, secondary or back-scattered electrons are emitted and detected. Morphology and particle dispersion were analyzed using an SEM-Quanta 450. Energy-Dispersive x-ray Spectroscopy (EDX), based on interactions between the sample and x-ray excitation, is used for elemental and chemical analysis. The chemical composition of the resulting nanostructures was analyzed using EDX within the SEM framework.

4. Result and discussion

4.1. UV–vis analysis of plant extract

The UV–vis spectroscopy analysis of the Thymus Kotschyanus plant extract was conducted across a wavelength range of 200 nm to 600 nm. The observed absorbance profile indicates the presence of various phytochemical compositions, including molecules characterized by n-electrons, σ-bonds, π-bonds, functional groups, chromophores, and aromatic rings [39]. The presence of two specific absorption peaks at 266 nm and 336 nm has been identified, likely corresponding to $n \rightarrow \pi^*$ and $n \rightarrow \sigma^*$ transitions. These peaks substantiate the existence of organic chromophores and phytochemicals such as thymol and carvacrol within the extract [40], with thymol noted for its significant bioactivity [39]. To further validate and detail the extract's characterization, it is recommended to complement the UV–vis analysis with advanced techniques like Gas Chromatography–Mass Spectrometry (GC-MS) and High-Performance Liquid Chromatography (HPLC) [40, 41]. Such a comprehensive investigation paves the way for utilizing these phytochemicals in the synthesis of nanomaterials, leveraging their reduction, capping, and stabilization capabilities.

4.2. UV–vis analysis of ZnO NPs

UV–vis absorption spectroscopy was employed to scrutinize the optical characteristics of ZnO nanoparticles (NPs). This technique, often utilized to affirm the creation of NPs, revealed the UV–vis absorption spectra of the ZnO NPs synthesized through biological means, as illustrated in figure 5. An excitation wavelength measuring 385 nm was recorded for the prepared ZnO NPs, aligning with the findings documented in existing literature [42, 43]. This wavelength corresponds to the band gap energy (E) of the material, signifying the amount of energy needed to promote an electron from the valence to the conduction band. The comprehension of this band gap energy is pivotal in elucidating the ZnO material's electrical and optical features. The optical bandgap of the ZnO NPs was ascertained using Tauc extrapolation, a process that consists of extending the linear part of the curve on a graph of $(\alpha h\nu)^2$ against $h\nu$, as demonstrated in figure 4 [44]:

$$(\alpha h\nu)^2 = A(h\nu - E_g)^n \tag{12}$$

Here, the absorption coefficient is symbolized by α, while the photon energy is denoted by $h\nu$. Additionally, A is a dimensionless constant, E_g signifies the energy of the bandgap, and the value of n corresponds to the transmission type, being equal to 1/2 for allowed direct transmission.

The UV–vis spectra analysis (refer to figure 5) provides explicit evidence of how ammonium hydroxide influences the creation of ZnO nanoparticles (NPs). Without ammonium hydroxide, the UV–vis spectra reveal an absorption peak at 421 nm, reflective of electronic transitions within the structural lattice of ZnO. However, the introduction of ammonium hydroxide leads to a discernible alteration in the absorption peak, shifting it to shorter wavelengths. Specifically, a sample containing 0.033 M of ammonium hydroxide demonstrates a peak at 349 nm, which corresponds to a blue shift when compared to a sample without ammonium hydroxide. This blue shift is indicative of a decrease in the size of the ZnO NPs, as tinier NPs generally exhibit a larger energy bandgap. Furthermore, an additional blue shift peak at 332 nm was detected in the sample with 0.335 M of ammonium hydroxide. This movement toward a shorter wavelength signifies the synthesis of even smaller ZnO NPs, characterized by an increased band gap energy.

These findings align well with the calculated band gap values obtained using the Tauc plot, as illustrated in figure 6.

Additionally, the UV–vis spectra of the fabricated ZnO NPs are impacted by the concentration of zinc nitrate hexahydrate. As demonstrated in figure 7, varying the concentration of this compound results in a pronounced

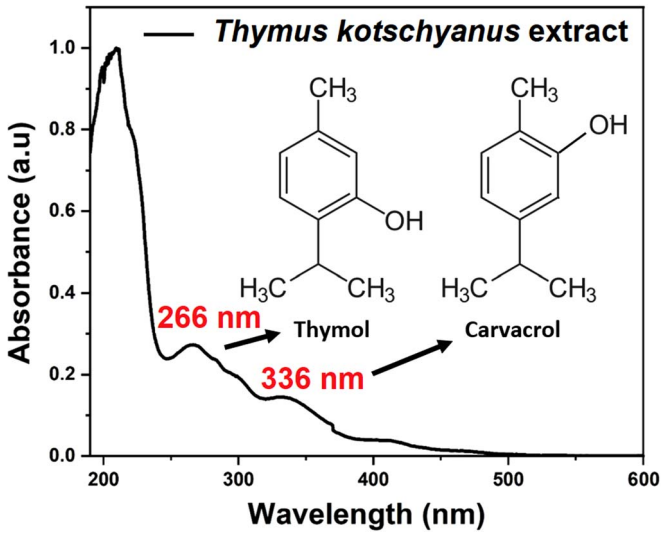

Figure 4. UV–vis spectroscopy of *Thymus Kotschyanus* plant extract.

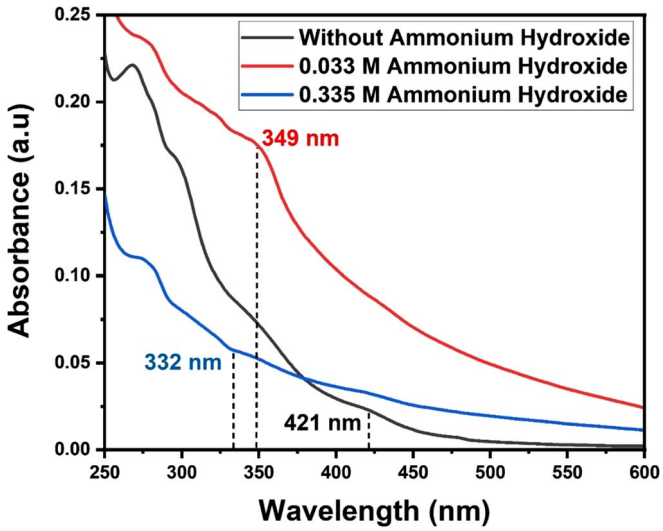

Figure 5. UV–vis spectra of ZnO seed layer grown using different ammonium hydroxide concentrations at RT.

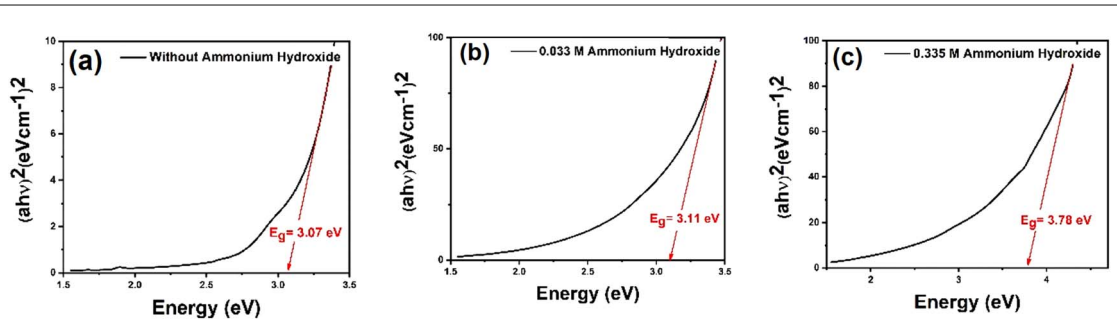

Figure 6. Energy bandgap measurement of ZnO NPs (a) without Ammonium hydroxide, (b) 0.033 M Ammonium hydroxide and (c) 0.335 M Ammonium hydroxide.

red shift in the absorption peak. More explicitly, an escalation in the concentration of zinc nitrate hexahydrate is associated with an enlargement of the NP size and a reduction in the band gap energy, as vividly illustrated in figure 8.

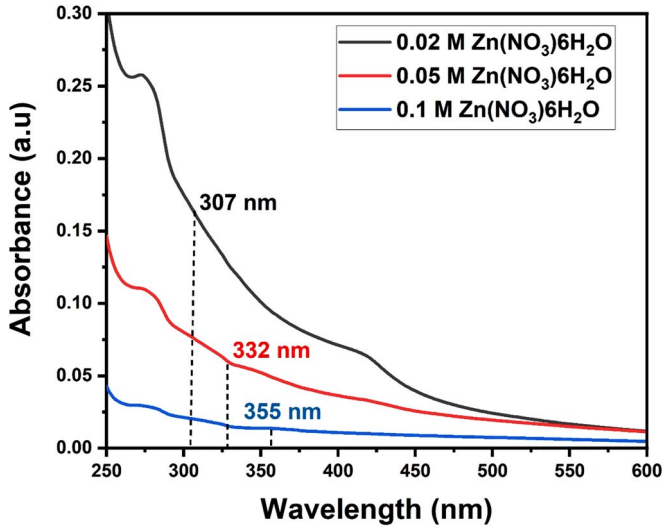

Figure 7. UV–vis spectra of ZnO NPs seed layer on glass substrate at different concentrations of zinc nitrate hexahydrate.

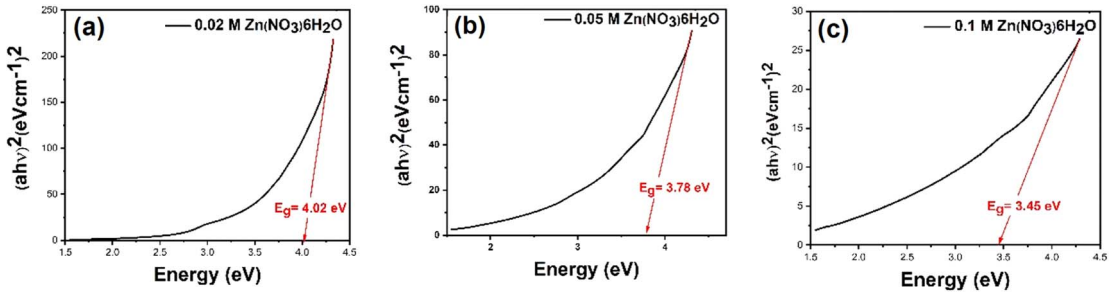

Figure 8. Energy bandgap measurement of ZnO NPs using (a) 0.02 M, (b) 0.05 M and (c) 0.1 M zinc nitrate hexahydrate.

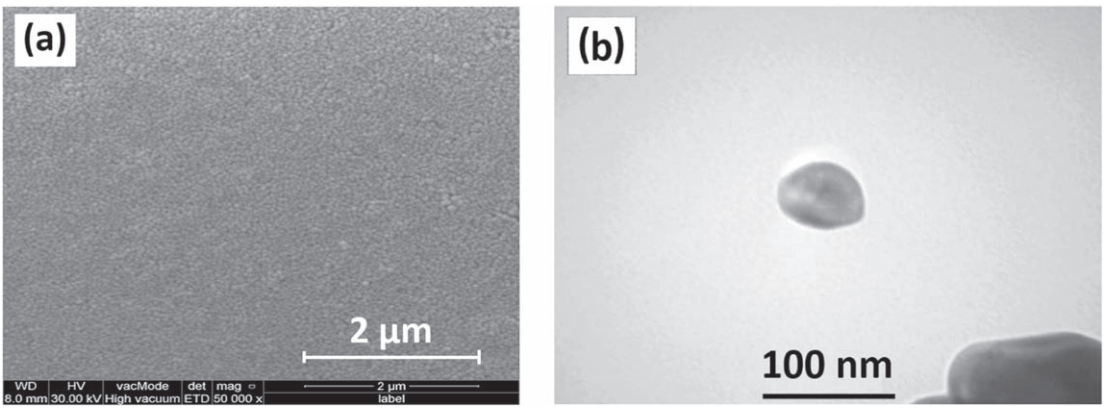

Figure 9. (a) SEM and (b) TEM images of the green synthesized ZnO NPs seed layer.

4.3. SEM, XRD and EDX analysis of ZnO seed layer grown by green synthesis

The surface characterization of ZnO seed layers on glass substrates were determined using SEM analysis. Figure 9(a) illustrates the obtained results after calcinating the ZnO seed layer at 450 °C, revealing a composed of small grains that are densely packed and exhibit minimal porosity. Furthermore, the nanoparticles are uniformly distributed across the glass substrate. The particle size of the seed layer plays a crucial role in determining the final structure of ZnO, as emphasized by previous studies [45, 46]. However, TEM analysis

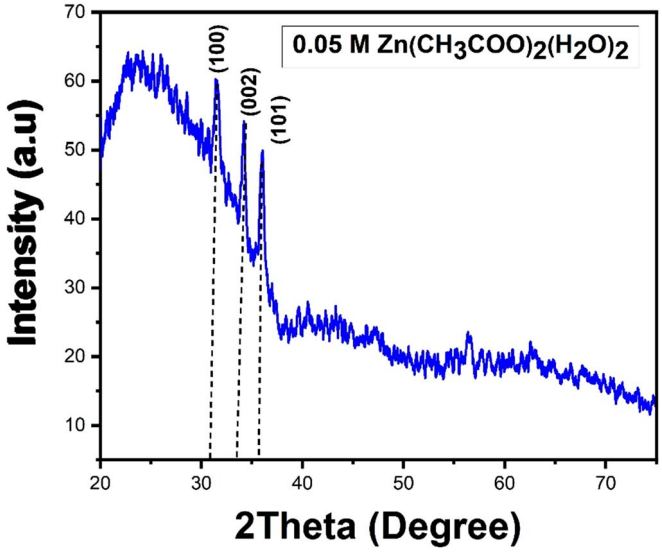

Figure 10. XRD spectrum from ZnO seed layer with concentration of 0.05 M ZAD.

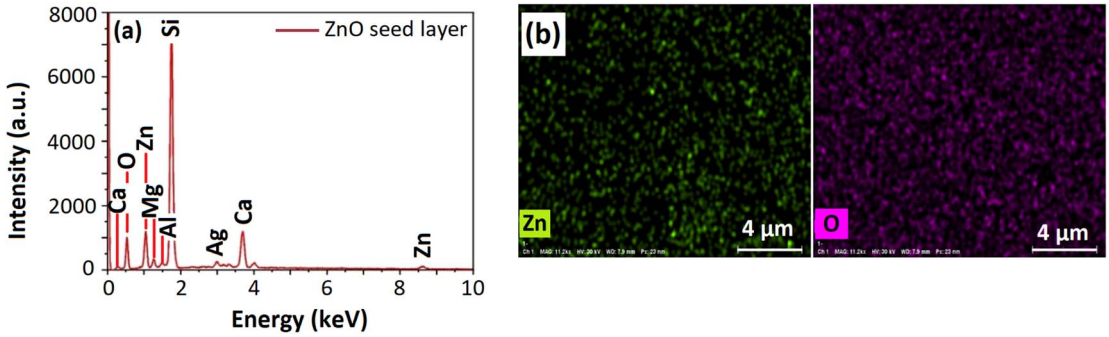

Figure 11. (a) EDX analysis and (b) elemental mapping distribution of Zn and O composition from ZnO seed layer.

demonstrates that the particles possess a nearly spherical shape, with an approximate nanoparticle size of 40 nm, as depicted in figure 9(b).

Figure 10 displays the x-ray diffraction spectra of ZnO nanoparticles (NPs) grown on a glass substrate. The intensity of the peaks corresponding to (100), (002), and (101) noticeably increases with higher deposition concentrations of zinc acetate dihydrate (ZAD) solution.

The elemental composition of ZnO NPs situated on a glass substrate was investigated using Energy Dispersive x-ray Spectroscopy (EDX). Figure 11(a) visually represents the distribution of ZnO seed layers, fabricated employing a green method. The study via EDX authenticated the presence of both oxygen (O) and zinc (Zn) atoms on the surface of the glass. Peaks corresponding to silver (Ag) were detected, a result of the application of a silver coating to augment the SEM image quality. Other elements, such as silicon (Si), calcium (Ca), aluminum (Al), magnesium (Mg), and sodium (Na), were also observed in the spectrum, attributed to the composition of the glass substrate. Furthermore, the EDX spectrum substantiated the purity of the ZnO seed layer. Comprehensive insights into the elemental composition, along with mapping distributions of zinc and oxygen atoms, are depicted in figure 11(b).

4.4. XRD analysis of ZnO NRs

To analyze the crystal structure and phase purity of the ZnO nanorods (NRs), x-ray diffraction (XRD) analysis was employed. The XRD patterns of the obtained samples are presented in figure 12. The growth of ZnO NRs on a glass substrate was conducted using different concentrations (0 M, 0.033 M, and 0.335 M) of ammonium hydroxide. For reference, the x-ray diffraction spectra of the glass substrate were also included as a base sample. Sample (a) exhibited a single broad peak, indicating the presence of an amorphous glass structure. In contrast, sample (b) displayed distinct diffraction peaks corresponding to the hexagonal wurtzite structure at (100), (002),

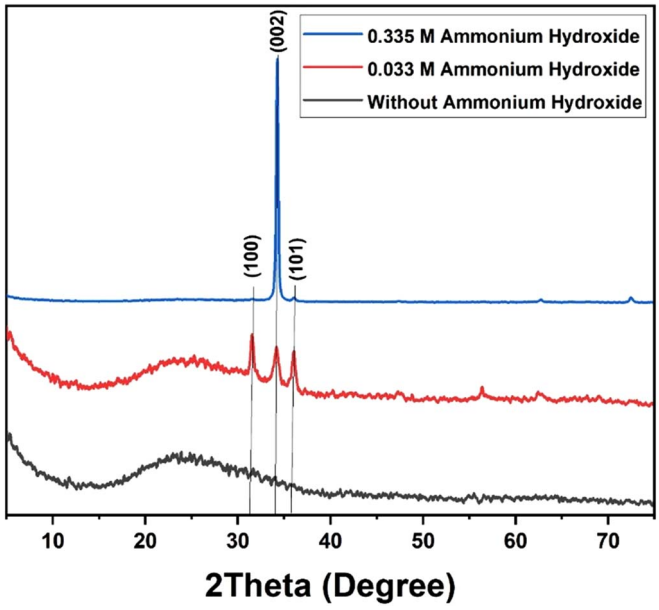

Figure 12. XRD spectrum from ZnO NRs grown at different (0, 0.033, 0.335) M of ammonium hydroxide concentrations.

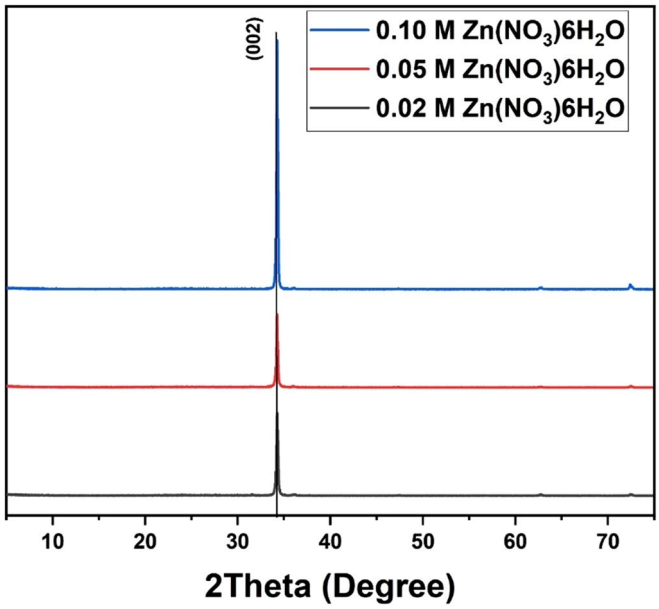

Figure 13. XRD spectrum from ZnO NRs grown at different (0.02, 0.05, 0.1) M of $Zn(NO_3)_2$ concentrations.

and (101). The intensity of these peaks increased as the concentration of the ammonia solution was raised to 0.335 M. Sample (c), synthesized at the highest concentration, i.e., 0.335 M of ammonium hydroxide, possesses the dominant peak of the *c*-axis. In this case the growth direction for the ZnO nanorods (NRs) was confirmed by the presence of the high intense (002) plane in the XRD analysis. The appearance of the highest intensity of the diffraction patterns for ZnO NRs validated their highly crystalline nature. Importantly, no foreign diffraction peaks corresponding to impurity phases were detected, signifying the formation of a pure ZnO phase.

Figure 13 illustrates the XRD pattern of ZnO samples grown at different concentrations of zinc nitrate hexahydrate (0.02, 0.05 and 0.1 M). The diffraction peaks in all samples indicate their nearly single-crystalline nature, with a preferential orientation along the *c*-axis of the hexagonal ZnO structure, specifically the (002) plane. The intensity of the (002) diffraction peak for ZnO is remarkably strong, indicating that the green-synthesized ZnO nanorods (NRs) were predominantly grown along the [001] direction. The XRD peaks observed in the samples consistently matched those listed in the standard ICSD Ref. Cod No. 98-006-5122, with

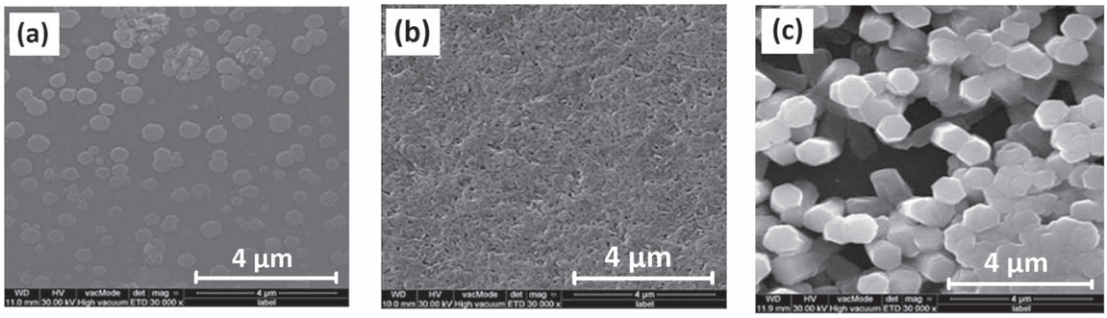

Figure 14. Growth with different amount of ammonium hydroxide, (a) without ammonium hydroxide, (b) 0.033 Mol ammonium hydroxide, (c) 0.335 Mol ammonium hydroxide.

Table 1. Crystalline size measurements of ZnO NRs using Debye–Scherrer's equation.

Sample	FWHM (^{0}2Theta)	Crystalline Size (nm)
Without Ammonium hydroxide	—	—
0.033 Mol Ammonium hydroxide	0.3149	26.4
0.335 Mol Ammonium hydroxide	0.0960	86.6
0.02 Mol Zinc nitrate hexahydrate	0.0984	84.8
0.05 Mol Zinc nitrate hexahydrate	0.0960	86.6
0.1 Mol Zinc nitrate hexahydrate	0.0960	86.6

no additional peaks corresponding to ZnO or other impurities detected. Among all the ZnO samples, the (002) plane exhibited the most intense peaks at $2\theta = 34.3°$, confirming the preferred growth direction along the *c*-axis due to its higher kinetic energy. This direction played a significant role in columnar growth compared to other planes. The average crystallite size of the ZnO nanoparticles was calculated using Debye–Scherrer's equation, as presented in table 1.

$$D = \frac{K\lambda}{\beta \cos\theta} \tag{13}$$

Where D is the crystal size, K is the shape factor (0.90), λ is the wavelength of x-ray diffraction ($\approx$0.15406 nm) for $Cu_{k\alpha}$, β is the full width at half maximum (FWHM) and θ is the diffraction angle [47]. Figures 12 and 13 demonstrate that increasing the precursor and ammonium hydroxide concentration does not cause a significant shift in the positions of the diffraction peaks. However, there is a noticeable increase in the intensity of these peaks. This can be attributed to a reduction in lattice disorder and a decrease in strain, both of which contribute to higher crystal quality at higher concentrations [48].

4.5. Morphology of ZnO NRs grown by green synthesis

Figure 14 illustrates the top and cross section view of ZnO NRs growth on glass substrates using different concentrations of ammonium hydroxide as an additive in the growth solution. In figure 14(a), where no ammonium hydroxide is added (0 M), the ZnO exhibits a nanodroplet-like morphology on the substrate. However, when 0.033 Mol of ammonium hydroxide is introduced, the SEM images in figure 14(b) reveal the formation of homogeneous nanopillar-like structures randomly oriented in different directions on the glass substrate. Furthermore, at the highest ammonium hydroxide concentration of 0.335 Mol, figure 14(c) shows that the obtained ZnO morphology is predominantly hexagonal in shape and perfectly aligned perpendicular to the growth surface. The addition of ammonium hydroxide during the synthesis process has a significant impact on the nucleation and growth rate of ZnO, influencing the formation of crystal structure and morphology. This effect is attributed to the supersaturation that affects nucleation formation [49]. Alenezi *et al* have explained the variation in ZnO nanowire density on an Au surface by stating that in the absence of ammonium hydroxide, primarily Zn^{2+} ions are available. In contrast, when ammonium hydroxide is used, their availability is limited, leading to a decrease in the rate of homogeneous nucleation and an increase in heterogeneous nucleation [50].

The lengths of the NRs increase steadily from 1.108 μm to 2.4 μm when the growth concentration was further increased from 0.001 to 0.02 M, whereas their diameters are found to be almost constant around 600 nm. Anisotropic crystal growth is essential for the creation of ZnO NRs. SEM images shown particles are almost perfectly aligned, with the nanoparticles epitaxially fused in a fixed orientation, which is the (002) plane, as

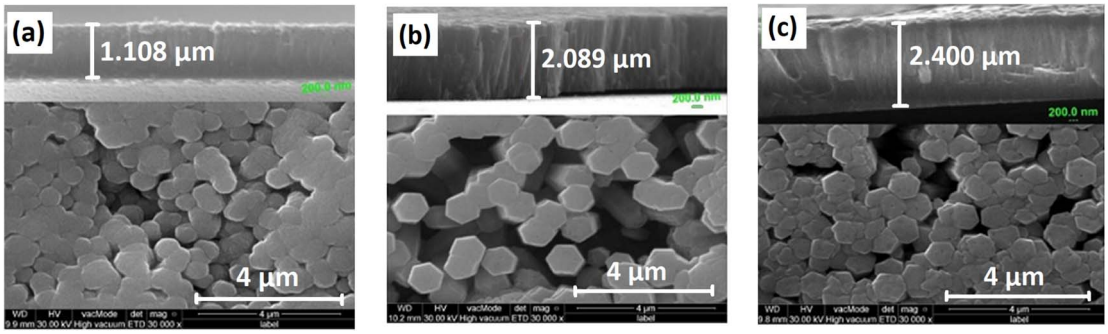

Figure 15. SEM images of top view and cross-section of green synthesized ZnO NRs grown using at. (a)0.02 M, (b) 0.05 M, (c) 0.1 M of zinc nitrate hexahydrate growth solution.

demonstrated by Pacholski *et al* they also, shown that ZnO NR development requires oriented attachment of ZnO NPs [38]. Thus, morphology of ZnO NRs and structural characteristics are influenced by the morphology of the ZnO seed layer [51]. Therefore, it can be concluded that in this work the most optimum growth parameters were determined to be 1 M of zinc concentration and 0.335 Mol of ammonium hydroxide as an additive solution, leading to the growth of well-aligned and hexagonal structure ZnO nanorod.

Figure 15 depicts both the top and cross-sectional views of synthesized ZnO nanorods (NRs) on glass substrates. The ZnO samples were grown using different concentrations of zinc nitrite solutions, namely (a) 0.001 M, (b) 0.01 M, and (c) 0.02 M, while maintaining the ammonium hydroxide concentration at 0.335 M. Across all three samples, the nanorods exhibit a predominantly vertical alignment along the *c*-axis direction. Sample (a) displays the lowest nanorod thickness, approximately 1.108 μm, and a significant amount of nanorod agglomeration. In sample (b), the nanorods exhibit a higher thickness of 2.089 μm compared to sample (a), but a lower nanorod density. Moreover, sample (b) demonstrates a well-defined hexagonal wurtzite structure compared to the other samples. In sample (c), the nanorods have the longest length at 2.4 μm and exhibit more pronounced agglomeration and higher density than sample (b). Despite identical growth parameters such as growth time, temperature, pH values, and plant extract concentration, sample (b), grown at a zinc nitrate hexahydrate concentration of 0.05 M, appears to be more favorable compared to the other samples. This preference is attributed to the presence of fewer combined nanorods and more clearly defined hexagonal shapes in sample (b) compared to samples (a), (c). Similar observations have been reported by S. Rajamanickam *et al* [51].

Figure 16 provides a detailed analysis of the elemental composition of ZnO nanorods (NRs) prepared using a green synthesis method at different growth concentrations. This analysis was conducted using an energy dispersive x-ray spectroscope (EDX) attached to the SEM machine. The EDX spectrum exhibited distinct peaks corresponding to Zn and O elements, indicating a high purity of ZnO during the growth process, with almost no impurities. The atomic percentage of Zn element in the Zn-O compound increased across all samples fabricated at different growth precursor concentrations, as depicted in the inset tables of figure 16. However, at higher growth concentrations, there was a noticeable increase in the Zn percentage and a corresponding decrease in the O percentage within the Zn-O compound. This phenomenon can be attributed to the greater availability of Zn atoms during the growth process at higher concentrations.

The elemental distributions of ZnO nanorods grown at various Zn salt concentrations were studied by EDX analysis, as shown in figure 17. The elemental mapping results show that the Zn and O elements are evenly distributed throughout all the ZnO samples.

5. Conclusion

In the current study, stable and aligned ZnO nanorods (NRs) on a glass substrate were successfully prepared by a novel green route using aqueous *Thymus kotschyanus* plant extract. The utilized procedure is rather simple, rapid, cheap, ecological and did not necessitate any organic solvents or other toxic reagents. Thus, we believe that the synthesis procedure is beneficial over conventional methods and open a wide door towards other NRs preparations. This study, also, highlights the significant influence of ammonium hydroxide and zinc precursor concentrations on the morphology and alignment of the green synthesized ZnO NRs. It has been shown that higher concentrations of ammonium hydroxide led to the formation of highly crystalline and well-aligned hexagonal ZnO NRs. Comprehensive analyses were conducted to investigate the morphology, structure, and optical characteristics of the biosynthesized ZnO NRs. Scanning electron microscopy analysis revealed an

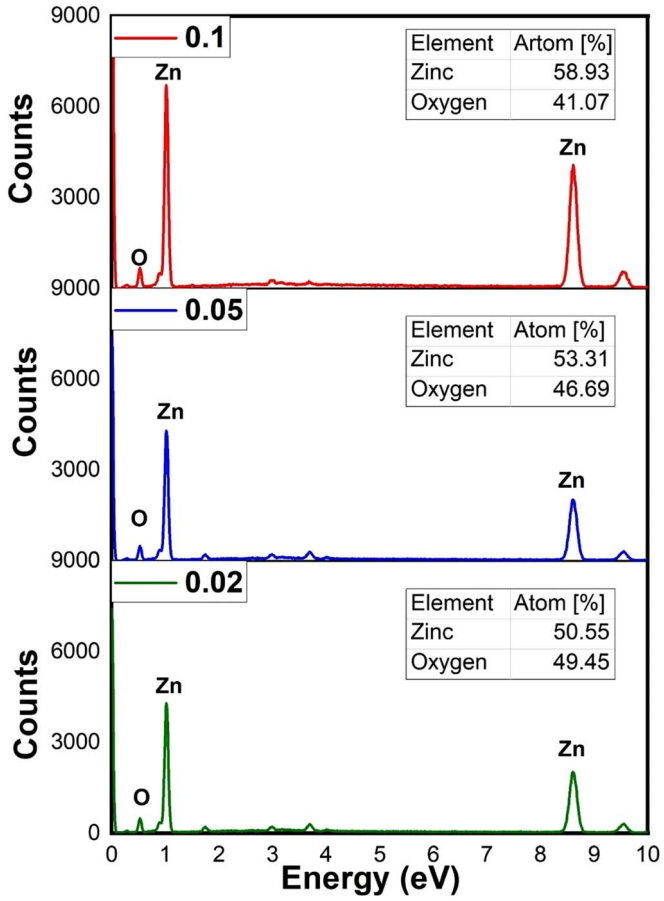

Figure 16. EDX spectrum of green synthesized ZnO NRs grown at (a) 0.02 M, (b) 0.05 M, (c) 0.1 M of Zinc nitrate hexahydrate growth solution.

increase in the average length of nanorods as the precursor concentration was raised. X-ray analysis consistently indicated the dominant of the (002) orientation in the ZnO patterns. Furthermore, the UV–vis spectrum study demonstrated an increase in average absorption intensity with higher concentrations of ammonium hydroxide. From our perspective, ZnO NRs could be one of the most significant nanomaterials in future research and applications. Therefore, the proposed novel method contributes to the understanding of ZnO NR synthesis and highlights the potential of green methods for the development of nanostructures.

Acknowledgments

The authors would like to acknowledge Soran University, for their unlimited supports. A superior acknowledge goes to Dr David M Waswa at Tishk International University for his outstanding proofreading of this manuscript.

Data availability statement

All data that support the findings of this study are included within the article (and any supplementary files).

Ethical approval

Not applicable.

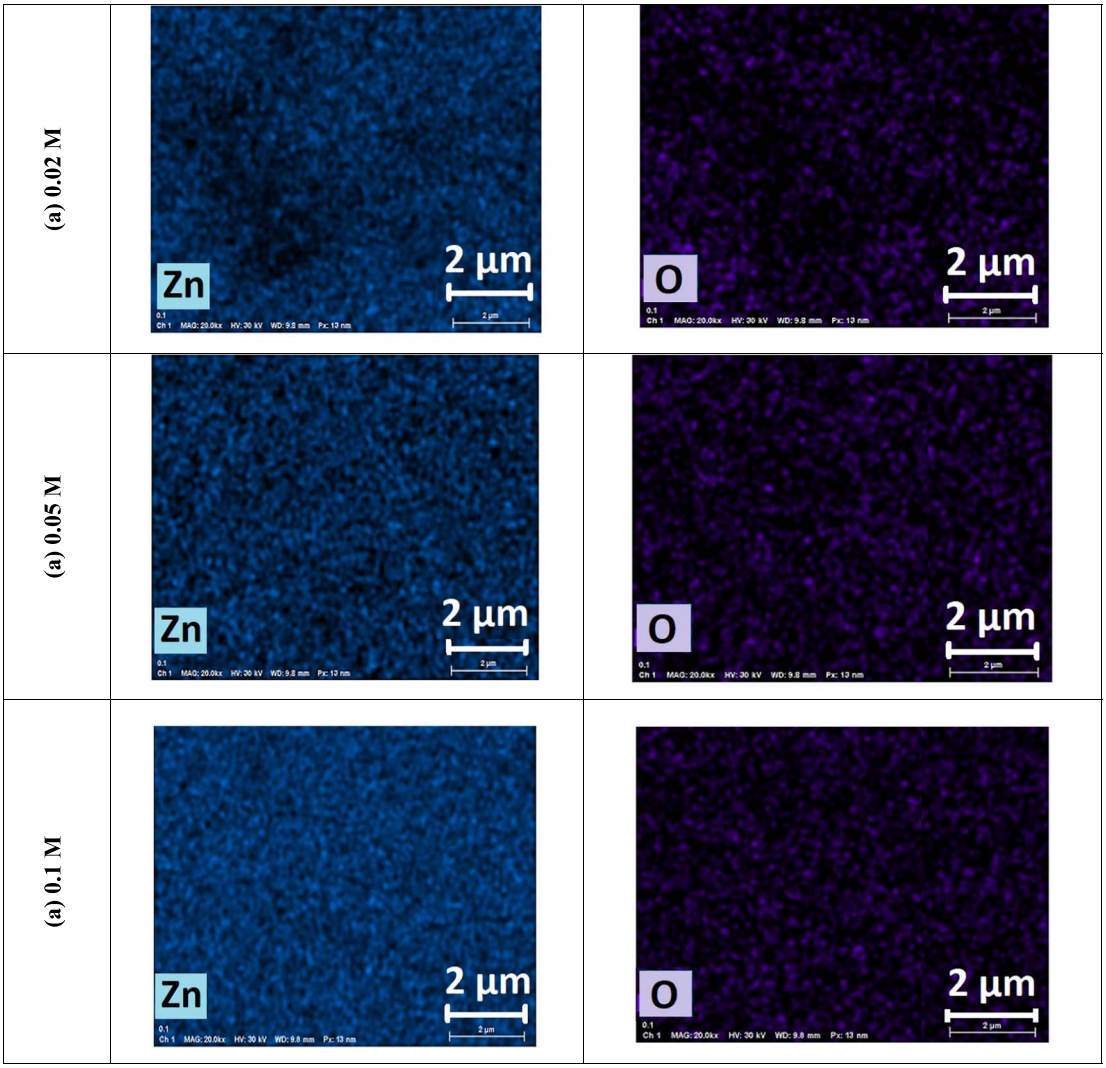

Figure 17. Zn and O elemental mapping distribution throughout green synthesized ZnO NRs at different concentrations (a) 0.02 M, (b) 0.05 M, and (c) 0.1 M of Zinc nitrate hexahydrate growth solution.

Authors' contributions

P K A: Methodology, data curation, plotting the graphs and writing—original draft preparation. A A B: Supervision, conceptualization, interpretation of results, writing-review /editing and submission. S M H: Methodology, data curation, and writing—original draft preparation.

Conflict of interest

The authors report no conflicts of interest.

Funding

This research received no external funding.

ORCID iDs

Azeez A Barzinjy https://orcid.org/0000-0003-4009-9845

References

[1] Barzinjy A A and Azeez H H 2020 Green synthesis and characterization of zinc oxide nanoparticles using eucalyptus globulus labill. leaf extract and zinc nitrate hexahydrate salt *SN Applied Sciences* **2** 1–14
[2] Barzinjy A A *et al* 2020 Biosynthesis, characterization and mechanism of formation of ZnO nanoparticles using petroselinum crispum leaf extract *Curr. Org. Synth.* **17** 558–66
[3] Barzinjy A A *et al* 2020 Biosynthesis and characterisation of zinc oxide nanoparticles from Punica granatum (pomegranate) juice extract and its application in thin films preparation by spin-coating method *Micro & Nano Letters.* **15** 415–20
[4] Franco M A *et al* 2022 A review on chemiresistive ZnO gas sensors *Sensors and Actuators Reports* **4** 100100
[5] Tsai Y-S *et al* 2021 Organic/inorganic hybrid nanostructures of polycrystalline perylene diimide decorated ZnO nanorods highly enhanced dual sensing performance of UV light/CO gas sensors *Results in Physics* **24** 104173
[6] Villarreal C C *et al* 2022 Graphene compared to fluorine-doped tin oxide as transparent conductor in ZnO dye-sensitized solar cells *J. Environ. Chem. Eng.* **10** 107551
[7] Lin Q *et al* 2022 Influence of annealing temperature on optical properties of sandwiched ZnO/Metal/ZnO transparent conductive thin films *Micromachines* **13** 296
[8] Zhang H *et al* 2022 Understanding the enhancement mechanism of ZnO nanorod-based piezoelectric devices through surface engineering *ACS Appl. Mater. Interfaces* **14** 29061–9
[9] Park C *et al* 2023 Supersonically sprayed self-aligned rGO nanosheets and ZnO/ZnMn2O4 nanowires for high-energy and high-power-density supercapacitors *Journal of Materials Science & Technology* **137** 193–204
[10] Ba M *et al* 2023 Controlling of hysteresis by varying ZnO-nanoparticles amount in P3HT: ZnO hybrid thin-film transistor: modeling *J. Electron. Mater.* **52** 1203–15
[11] He Y *et al* 2023 ZnO/SiO_2 encapsulation of perovskite nanocrystals for efficient and stable light-emitting diodes *Appl. Surf. Sci.* **611** 155724
[12] Wang Y *et al* 2023 New method for preparing ZnO layer for efficient and stable organic solar cells *Adv. Mater.* **35** 2208305
[13] Guo T *et al* 2015 A comprehensive review on synthesis methods for transition-metal oxide nanostructures *Cryst. Eng. Comm.* **17** 3551–85
[14] Panda D and Tseng T-Y 2013 One-dimensional ZnO nanostructures: fabrication, optoelectronic properties, and device applications *J. Mater. Sci.* **48** 6849–77
[15] Xia Y *et al* 2003 One-dimensional nanostructures: synthesis, characterization, and applications *Adv. Mater.* **15** 353–89
[16] Wu X *et al* 2011 Low temperature growth and properties of ZnO nanorod arrays. Advances in Natural *Sciences: Nanoscience and Nanotechnology* **2** 035006
[17] Mahmood, M A and Dutta J 2011 Spray pyrolized pre-coating layers for controlled growth of zinc oxide nanorods by hydrothermal process *Nanoscience & Nanotechnology-Asia* **1** 92–6
[18] Jabeen M, Vasant Kumar R and Ali N 2020 A review on preparation of ZnO nanorods and their use in ethanol vapors sensing *Gas Sensors* 1–24
[19] Al-Rasheedi A *et al* 2022 Influence of salt solution concentration on structural properties of ZnO nanorods grown by hydrothermal method *Appl. Phys.* A **128** 782
[20] Radičić R *et al* 2022 Synthesis of silver, gold, and platinum doped zinc oxide nanoparticles by pulsed laser ablation in water *Nanomaterials* **12** 3484
[21] Aspoukeh P K, Barzinjy A A and Hamad S M 2022 Synthesis, properties and uses of ZnO nanorods: a mini review *International Nano Letters* **12** 153–68
[22] Pourshaban E, Abdizadeh H and Golobostanfard M R 2016 A close correlation between nucleation sites, growth and final properties of ZnO nanorod arrays: sol-gel assisted chemical bath deposition process *Ceram. Int.* **42** 14721–9
[23] Azmi Z H *et al* 2022 Effect of seed layer on the growth of zinc oxide nanowires by chemical bath deposition method *Coatings* **12** 474
[24] Wu W *et al* 2008 Epitaxy of vertical ZnO nanorod arrays on highly (001)-oriented ZnO seed monolayer by a hydrothermal route *Cryst. Growth Des.* **8** 4014–20
[25] Hasnidawani J *et al* 2016 Synthesis of ZnO nanostructures using sol-gel method *Procedia Chem.* **19** 211–6
[26] Guo X-L *et al* 2001 Fabrication and optoelectronic properties of a transparent ZnO homostructural light-emitting diode *Jpn. J. Appl. Phys.* **40** L177
[27] Wagner A R and Ellis S W 1964 Vapor-liquid-solid mechanism of single crystal growth *Appl. Phys. Lett.* **4** 89–90
[28] Vanitha G *et al* 2022 Review on green synthesis of nanoparticles using various strong electrolytic metal solutions mediated by various plant parts *Journal of Nanoscience and Technology* 960–6
[29] Greene L E *et al* 2003 Low-temperature wafer-scale production of ZnO nanowire arrays *Angew. Chem.* **115** 3139–42
[30] Ghasemi Pirbalouti A, Emami Bistghani Z and Malekpoor F 2015 An overview on genus thymus *Journal of Medicinal Herbs* **6** 93–100
[31] Stahl-Biskup E 1991 The chemical composition of thymus oils: a review of the literature 1960–1989 *J. Essent. Oil Res.* **3** 61–82
[32] Golkar P, Mosavat N and Jalali S A H 2020 Essential oils, chemical constituents, antioxidant, antibacterial and in vitro cytotoxic activity of different thymus species and zataria multiflora collected from Iran *S. Afr. J. Bot.* **130** 250–8
[33] Zare M *et al* 2019 Biocompatibility assessment and photocatalytic activity of bio-hydrothermal synthesis of ZnO nanoparticles by Thymus vulgaris leaf extract *Mater. Res. Bull.* **109** 49–59
[34] Weldegebrieal G K 2020 Synthesis method, antibacterial and photocatalytic activity of ZnO nanoparticles for azo dyes in wastewater treatment: a review *Inorg. Chem. Commun.* **120** 108140
[35] Nazir A *et al* 2020 Evaluation of source, depositional environment, thermal maturity and biodegradation of organic matter from kohat-potwar basin, Pakistan *Pet. Sci. Technol.* **38** 106–15
[36] Yadav A B, Parvathi P V and Thabassum S R 2019 Effect of precursor chemistry on the structural and sensing properties of hydrothermally grown nanorods *Appl. Phys.* A **125** 1–9
[37] Li Q *et al* 2005 Fabrication of ZnO nanorods and nanotubes in aqueous solutions *Chem. Mater.* **17** 1001–6
[38] Abdulrahman A F, Abd-Alghafour N and Ahmed S M 2021 Optimization and characterization of SILAR synthesized ZnO nanorods for UV photodetector sensor *Sens. Actuators* A **323** 112656
[39] Doosti M-H, Ahmadi K and Fasihi-Ramandi M 2018 The effect of ethanolic extract of Thymus kotschyanus on cancer cell growth in vitro and depression-like behavior in the mouse *Journal of Traditional and Complementary Medicine* **8** 89–94
[40] Rajkumar P *et al* 2018 Vibrational and electronic spectral analysis of thymol an isomer of carvacrol isolated from Trachyspermum ammi seed: a combined experimental and theoretical study *Chemical Data Collections* **15** 10–31

[41] Karpagasundari C and Kulothungan S 2014 Analysis of bioactive compounds in physalis minima leaves using GC MS, HPLC, UV–vis and FTIR techniques *Journal of Pharmacognosy and Phytochemistry* **3** 196–201
[42] Fakhari S, Jamzad M and Kabiri H 2019 Fard, Green synthesis of zinc oxide nanoparticles: a comparison. *Green Chem. Lett. Rev.* **12** 19–24
[43] Moghaddas S M T H, Elahi B and Javanbakht V 2020 Biosynthesis of pure zinc oxide nanoparticles using quince seed mucilage for photocatalytic dye degradation *J. Alloys Compd.* **821** 153519
[44] Mohammad S M *et al* 2015 Fabrication of low cost UV photo detector using ZnO nanorods grown onto nylon substrate *J. Mater. Sci., Mater. Electron.* **26** 1322–31
[45] Wu W Y, Yeh C C and Ting J M 2009 Effects of seed layer characteristics on the synthesis of ZnO nanowires *J. Am. Ceram. Soc.* **92** 2718–23
[46] Ghayour H *et al* 2011 The effect of seed layer thickness on alignment and morphology of ZnO nanorods *Vacuum* **86** 101–5
[47] Vijayalakshmi R and Rajendran V 2012 Synthesis and characterization of nano-TiO2 via different methods *Archives of Applied Science Research* **4** 1183–90
[48] Yadav A B, Parvathi P and Shaik R T 2019 Zero bias UV detection and precursor effect on properties of ZnO nanorods grown by hydrothermal method on SiO2/p-Si substrate *Thin Solid Films* **685** 343–52
[49] Dahiya A S *et al* 2018 Photoluminescence study of the influence of additive ammonium hydroxide in hydrothermally grown ZnO nanowires *Nanoscale Res. Lett.* **13** 1–9
[50] Alenezi M R, Henley S J and Silva S 2015 On-chip fabrication of high performance nanostructured ZnO UV detectors *Sci. Rep.* **5** 1–9
[51] Rajamanickam S, Mohammad S M and Hassan Z 2022 *Colloid and Interface Science Communications* **47** 100588